

Comparison of different sparse dictionaries for compressive sampling

Deepak M. Devendrappa¹, Karthik P.², Deepak N. Ananth³, Aruna Kumar P.⁴

¹Department of Computer Science and Engineering, K S School of Engineering and Management, Bengaluru, India

²Department of Electronics and Communication Engineering, K S School of Engineering and Management, Bengaluru, India

³Department of Computer Science and Engineering, R V Institute of Technology and Management, Bengaluru, India

⁴Department of Information Science and Engineering, JNN College of Engineering, Shivamogga, India

Article Info

Article history:

Received May 10, 2022

Revised Jun 10, 2022

Accepted Jul 16, 2022

Keywords:

Compressed sensing

CoSaMP

Dictionary learning

Magnetic resonance imaging

Nyquist theorem

ABSTRACT

Compressive sampling/compressed sensing (CS) is building on the observation that most of the signals in nature are sparse or compressible concerning some transform domain. And by converse, the same can be reconstructed with high accuracy by making use of far fewer samples than what is required by violating Shannon-Nyquist theorem. Some of the transform techniques are discrete cosine transform, fast fourier transforms discrete wavelet transform, discrete fourier transforms. In this paper, novel CS techniques are FFTCoSaMP, DCTCoSaMP, and DWTCoSAMP are introduced and compared on different sparse transforms for CS in magnetic resonance (MR) images based on sparse signal sequences/dictionaries by means of transform techniques with respect to objective quality assessment algorithms like PSNR, SSIM and RMSE, where CoSaMP stands for compressive sampling matching pursuit. DWTCoSAMP is giving the PSNR values of 37.16 (DB4), 38.12 (Coif3), 38.5 (Sym8), for DCTCoSaMP and FFTCoSaMP, it's 36.33 and 36.01 respectively. For DWTCoSAMP, SSIM value is 0.81, and for DCTCoSaMP and FFTCoSaMP, it's 0.73 and 0.7 respectively. And finally, for DWTCoSAMP, RMSE value is 0.66, and for DCTCoSaMP and FFTCoSaMP, it's 0.53 and 0.41 respectively. DWTCoSAMP reveals the best than rest of the methods and traditional CS techniques by the detailed comparison and analysis.

This is an open access article under the [CC BY-SA](https://creativecommons.org/licenses/by-sa/4.0/) license.



Corresponding Author:

Deepak M. Devendrappa

Department of Computer Science and Engineering, K S School of Engineering and Management

Holiday Village Road, Mallasandra, Kanakapura Rd, Bengaluru, Karnataka 560109, India

Email: mddeepak1986@gmail.com

1. INTRODUCTION

A signal can be completely rebuilt using a linear reconstruction method if it is sampled at equal intervals and bandlimited by less than the sampling rate. The frequency range and sample rate spanned by the signal are used to reconstruct the signal. The signals can be captured and modeled by several mathematical approaches. One such kind of approach is the compressed sensing (CS) technique [1]-[8]. CS assumes the signal to be sparse. For a two-dimensional signal, most of the entries in its vector space are zeros. So, it is called as sparse vector space for limited dimensional signal. Sparse vector doesn't have itself to be consist of signal of interest but it can be equally well represented by some basic functions like wavelet or fourier transforms.

Let's consider a set of vectors $\{x\}$ that are linearly dependent and if there are scalars that not at all zeros is given by $(1) \sum_i \lambda_i x_i = 0$. Then set of vectors $\{x_i\}$ are linearly independent and orthogonal. If the inner product of any two vectors in the set is zero, then it is called orthogonal. Sparsity is an important and more

powerful concept in the field of mathematics and computer science. Consider an N-dimensional x, it can be expressed by a linear super position of $K \ll N$ elementary signal quantities for some error e and $e(k)$ called sparse for the vector α . K quantize ψ_k are collected from a dictionary in turn which is represented by N x D matrix with $D \gg N$ [2].

$$x = \sum_{k=1}^K \alpha_k \psi_k \text{ in } \|x - x_k\|_2 \leq e(k) \tag{1}$$

The exact sparsity can be represented by $y = \Psi x$, [9]-[11] where Ψ is an orthonormal basis, x is the input signal. Some of the dictionary representations are fast fourier transforms (FFT), discrete cosine transform (DCT), and discrete wavelet transform (DWT). FFT [12] of the signal x_k of the signal y_k is given by (2).

$$X_k = 1/\text{sqrt}(n) \sum_{j=1}^N Y_k \exp(-2\pi(j-1)(k-1)i/N) \tag{2}$$

By assuming the sparse version of signal X [13] in which all significant entries are set to zero. We can use this sparse vector Z to approximate the original signal. $\delta Y = Y - \bar{Y} = \bar{F}(X - Z)$ we can make of Z to approximately predict y. $Z \rightarrow \bar{Y} \approx Y \rightarrow y$. As we know the locations of non-vanishing entries in the sparse vector, only fractions of samples in Y are used to recreate Z [14] as in (3).

$$\text{Then } y^m = \bar{F}_{m \times m} Z^m = \bar{F}_{m \times N} Z \tag{3}$$

Where $y^m \in R^m$, $Z^m \in R^m$, $F_{m \times m} \in R^{m \times m}$, $\bar{F}_{m \times N} \in R^{m \times N}$. are got by removing the rows/columns of the vanishing entries in Z. And so, we can recreate by sampling $m < N$ points at specific locations which may go faraway less than the Nyquist rate [15]. $y^m = \bar{F}_{m \times N} Z$, in which the sample in Z are less than the length of the sparse vector. The relationship between the discrete representation of y and fourier transform is given by $X = FY$ where F being the DFT dictionary, $X = \{X_k\}_{k=1}^N \in R^n$ and $Y = \{Y_k\}_{k=1}^N \in R^n$. The inverse way of producing the signal $Y = \bar{F}X$, where \bar{F} is transpose of the F (inverse of DFT) and X is called the compressible vector or sparse vector. In this case of signal X, the signal energy is not distributed equally over the spectrum. So, it is approximated by reduced representation. DCT [16] is considered as the discrete-time version of the fourier cosine series as shown mathematically (4). DCT estimates the real approximation of the signal with less coefficients.

$$D((i,j)) = (1/\sqrt{2N}) C(i), C(j) \sum_0^{M-1} \sum_0^{N-1} p(x,y) \cos[(2x+1)i\pi/2N] \cos[(2y+1)j\pi/2N] \tag{4}$$

Otherwise, $C(u) = C(v) = 1$. The pixel in the image represented by the M x N matrix is p (x, y). DCT is applied on a block of size N, and f(x, y) is the N x N input image. The encoded or transformed image of f(x,y) is F(u,v). DWT [17], [18] decomposes the signal into approximation and detailed subbands. The detailed subbands are having the much information about the image. They are called as high significant components of the signal. Approximate subbands are the least significant components of the mages. The least significant components are nothing but the edges present in the image. There are different types of wavelet families like. Haar, Dabhache, and symmetric. We have experimented with Haar wavelet transforms. The general wavelet transform is (5) and (6).

$$F_{High\ Pass}(m,n) = \int_{-\infty}^{\infty} f(x) \Psi_{(m,n)}^*(t) dt \tag{5}$$

$$F_{Low\ Pass}(m,n) = \int_{-\infty}^{\infty} f(x) \Phi_{(m,n)}^*(t) dt \tag{6}$$

High pass filter $F_{High\ Pass}(m,n)$ passes through high-frequency components and low pass filter $F_{Low\ Pass}(m,n)$ passes through low-frequency components. * is a conjugate symbol. In (5) represents the wavelet function given by Ψ and in (6) represents the scaling function given by Φ . f(x) is the input signal. The input signal is represented by f(x). The wavelet transform has some advantages: i) wavelet transforms at higher levels avoid blocking artifacts, ii) well matched to Herpes simplex virus (HSV) characteristics, and iii) wavelet provides higher level of decomposition.

Let A denote the m x N sampling matrix with the restricted isometry criterion (RIC) $\delta_2s \leq c$ [19]. Let consider a signal f that is sparse, x has only K non-zero entries. $f = \psi x$, where ψ is some transform domain [20], [21]. The measurement vector can be obtained as $y = \phi f = \phi \psi x = Ax$. A is called the measurement matrix and ϕ is called the sampling matrix. The sparse vector can be reconstructed by solving the linear equation $y = Ax$ [22]-[24].

2. PROPOSED METHODS

The compressive sampling matching pursuit (CoSaMP) [25], [26] is a compressed sensing technique based on orthogonal matching pursuit. It must fulfill the following requirements: i) it must begin with the least sample data possible. ii) It should progress by taking into account samples from various sampling strategies. iii) It must accept all samples that have been combined with noise and must be resilient. Novel CS techniques DCTCoSaMP, FFTCoSaMP, and DWTCoSAMP are proposed in this paper to recover the original signal from the sparse or incomplete signal components. Finally, using the peak signal-to-noise ratio (PSNR), structured similarity indexing method (SSIM) and root mean square error (RMSE) approaches, the restoration of magnetic resonance imaging (MRI) images is analyzed and compared.

2.1. Orthonormal bases

Assume set B . B has a set of vectors, viz. $B = \{v_1, v_2, \dots, v_k\}$, each of which has a length of 1. $\|v_i\| = 1$ for $i = 1, 2, \dots, k$. or $v_i \cdot v_j = 0$ for $i \neq j$. All of the vectors in B have a length of one, indicating that they all have been scaled and are unit vectors. Any two vectors in the collection have a dot product of zero, i.e. $v_i \cdot v_j = 0$ for i and j . These vectors are all orthogonal and have the same length and are normalized. As a result, set B is considered too as orthonormal. The term orthogonal points that all of the set's components are orthogonal and normalized.

CoSaMP is an orthogonal matching pursuit-based (OMP-based) encoding/decoding approach. Because of one of the compressed sensing techniques, CoSaMP has gotten a lot of interest today. The CoSaMP method accepts a K -sparse signal array as input. The measurement grid should be accepted. Finally, it should also accept the criterion for halting. The CoSaMP [27]-[29] is a greedy matching pursuit algorithm.

2.2. Algorithm CoSaMP (M, ϕ, s)

The algorithm begins with a basic signal approximation, in which the starting leftover signal equals the unknown target signal. It functions through 5 important phases throughout each iterative process: i) identification: from the available samples, the algorithm creates a substitute of the residual and locates the significant components of the substitute; ii) support merger: the newly discovered components are combined with the components found in the present estimation; iii) estimation: to estimate the target signal on the merged set of components, the method performs a least-squares problem; iv) pruning: by preserving just the biggest elements in this least-squares signal approximation, the method creates a new approximation; v) sample update: finally, the samples are updated to represent the residual signal, which is the portion of the signal that has not been estimated or approximated.

Figure 1 depicts the recommended architecture for the proposed approaches. The system receives an MRI image as input, and uses dictionary extraction methods including FFT, DCT, and DWT to leverage sparsity factors. The low and high-frequency components are included in the dictionary. Only low-frequency components, which signify incomplete or sparse components, are retained. Novel CS techniques DCTCoSaMP, FFTCoSaMP and DWTCoSAMP are proposed in this paper to recover the original signal from the sparse or incomplete signal components. Finally, using the PSNR, SSIM, and RMSE approaches, the restoration of MRI images is analyzed and compared.

```

Input: Significant coefficients to be selected  $M$ , random measurement matrix  $\Phi$ ,
sparsity level  $s$ .
Output: The target signal's  $s$ -sparse approximation
Initialisation:  $f_0 \leftarrow 0$  // initial approximation,  $y_0 \leftarrow y$  // Current samples = input
samples,  $t \leftarrow 0$ 
loop
1.  $t \leftarrow t + 1$  // Increase the number of cycles each time.
2.  $\delta \leftarrow M * y^0$  // Create a list of intermediates.
3.  $B \leftarrow \text{supp}(\delta_{2s})$  // Make a comprehensive collection of substitutes.
4.  $B^t \leftarrow B \cup \text{supp}(f^{t-1})$  // Promote a merger
5.  $b|_{B^t} \leftarrow (M_{T^t})^+ B^t$  // Least-squares signal estimate
6.  $b|_{B^c} \leftarrow 0$ 
7.  $f^t \leftarrow b_k$  // Shear/trim in order to get the next estimate
8.  $y^0 \leftarrow y - A f^t$  // Renew the samples:
till halting criterion holds
 $f \leftarrow f^t$ 

```

The block diagram for DCTCoSaMP/FFTCoSaMP/DWTCoSAMP as shown in Figure 2. The CoSaMP algorithm takes the input image, where it calculates the automatic correlation, it means, it selects only the sparsity features present in the signal. And it selects the current set of preselected atoms (only a few k non-zero coefficients). Then merge sparse vector with measurement matrix to form the candidate atom set. Then least square methods are used to get the signal residuals. Shear or prune to obtain the supporting atom set in order to get the better estimation. Update the current final estimate and calculate the current residuals until stopping

criteria is met. If stopping criteria is not met, update the current residual and support set. And the whole process continues further.

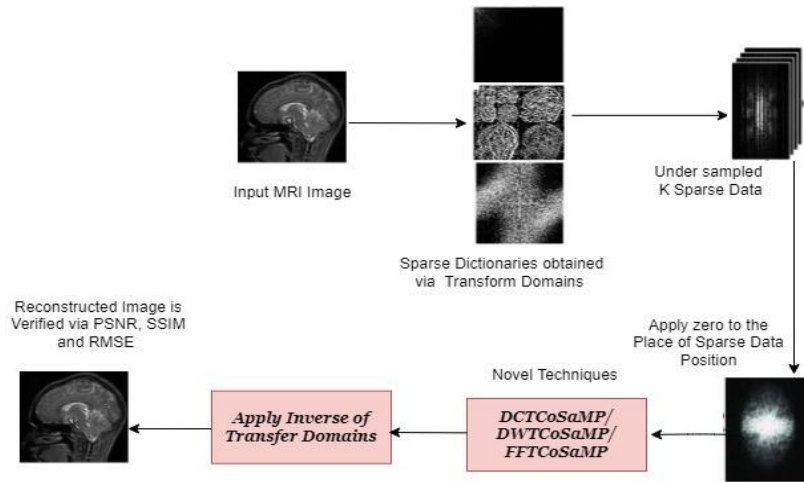


Figure 1. Architecture for the proposed methods

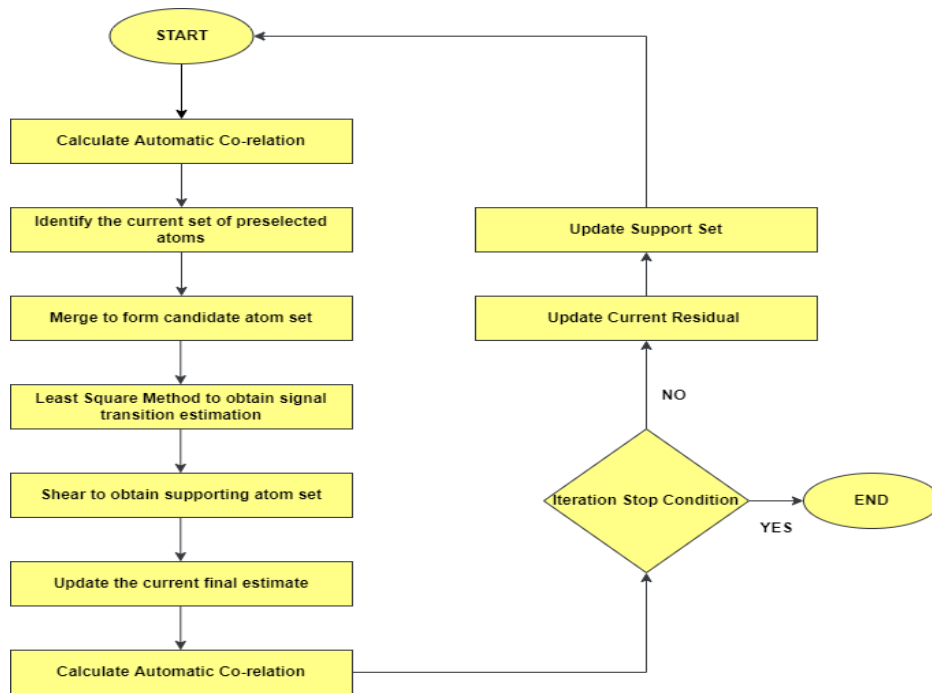


Figure 2. Block diagram for FTTCoSAMP/DCTCoSaMP/DWTCoSAMP

3. EXPERIMENTAL RESULTS

In this article, six different types of MRI images like Glioma Tumor images, Brain Tumor images, Brain Tumorless images, no Brain Tumor images, Non Cancerous images, and Cancerous images as shown in Figure 3. The experimentation is conducted on about 2,000 MRI images. The dataset has been taken from some websites like www.kaggle.com and the state-run Victoria hospital, Bengaluru. We have experimented on different dimensions of measurement matrices like 256x210, 256x180, and 256x155. Among all these dimensions of measurement matrices, the dimension 256x210 is exploiting the best reconstruction and acceptable measurement matrix. For the 256x210 measurement matrix, the comparative results for different CS

techniques like FFTCoSaMP, DCTCoSaMP, and DWTCoSAMP are tabulated and analyzed through experimentation methods.

Table 1 compares PSNR, SSIM, and RMSE values obtained from thorax MRI images and compared to some research articles using various compressed sensing approaches. The proposed methods FFTCoSaMP, DCTCoSaMP, and DWTCoSAMP provide better PSNR, SSIM, and MSE values than all of the references found in the literature review. The results of experimentation are tabulated.

CS technique has been discussed in various papers as per the references mentioned in [26], [30]-[33]. Where PSNR values for different CS techniques including CoSaMP algorithm are discussed as per the experiments from various researchers, it is observed that PSNR values for my proposed methods are higher than the other CS techniques of the literature survey. Similarly, SSIM values for different CS techniques including CoSaMP algorithm are discussed as per the experiments from various researchers. It is observed that SSIM values for my proposed methods are higher than the other CS techniques of the references [34]-[37]. Finally, RMSE values for different CS techniques, are discussed as per the experiments from various researchers. It is observed that RMSE values for my proposed methods are lower than the other CS techniques of the literature survey [34]-[38].

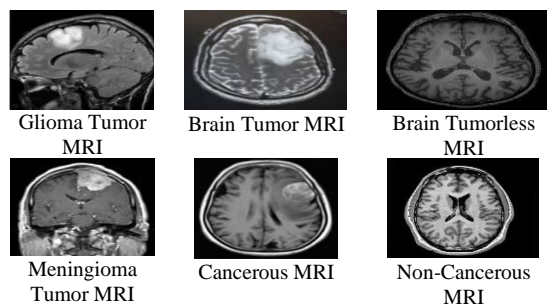


Figure 3. MRI images used for exploitation of various sparse dictionaries

Table 1. PSNR, SSIM, and RMSE values for the proposed methods

Objective quality assessments type	Proposed methods	Results
PSNR	FFTCoSAMP	36.01
	DCTCoSaMP	36.33
	DWTCoSAMP	37.16 (DB4) 38.12 (Coif3) 38.5 (Sym8)
SSIM	FFTCoSAMP	0.7
	DCTCoSaMP	0.73
	DWTCoSAMP	0.81
RMSE	FFTCoSAMP	0.66
	DCTCoSaMP	0.53
	DWTCoSAMP	0.41

Table 2 shows the comparison of different compressive sampling techniques w.r.t. PSNR, SSIM and RMSE for different MR images like Glioma Tumor images, Brain Tumor images, Brain Tumorless images, no Brain Tumor images, non Cancerous images, and Cancerous images. As mentioned, the experiment is conducted on 2,000 MRI of of different categories of Glioma-Tumor images, Brain Tumor images, Brain-Tumorless images, no_Brain_Tumor_images, non-Cancerous images, and Cancerous MR images. The average value of PSNR for all these images w.r.t. CS technique DWTCoSAMP is 33.0347, which is high when compared to other CS techniques like FFTDCoSAMP and DWTCoSAMP with PSNR values 26.6229 and 27.7749 respectively. Similarly, the average value of SSIM for all these images w.r.t. CS technique DWTCoSAMP is 0.6373, which is almost equivalent to SSIM value 0.7136 of FFTCoSaMP and 0.4506 of DCTCoSaMP. Lastly the average value of RMSE for all these images w.r.t. CS technique DWTCoSAMP is 0.0019, which is less when compared to other CS techniques like FFTCoSaMP and DCTCoSaMP with PSNR values 0.0451 and 0.0036 respectively.

Table 2. Comparison of different compressive sampling techniques w.r.t. PSNR, SSIM, and RMSE for measurement matrix of dimension 210 X 256

S N	Metrics MRI images	PSNR			SSIM			RMSE		
		FFTCoSAMP	DCTCoSaMP	DWTCoSAMP	FFTCoSAMP	DCTCoSaMP	DWTCoSAMP	FFTCoSAMP	DCTCoSaMP	DWTCoSAMP
1	Glioma Tumor images	26.7953	27.9552	32.9565	0.7021	0.4644	0.5938	0.0016	0.0019	0.0006
2	Brain Tumor images	26.1371	27.3214	32.7034	0.8534	0.4914	0.8423	0.2190	0.0021	0.0006
3	Brain Tumorless images	26.7877	27.7369	33.2316	0.4284	0.4251	0.5759	0.0016	0.0019	0.0006
4	No Brain Tumor images	26.9530	28.2062	33.3209	0.7264	0.4311	0.5891	0.0015	0.0053	0.0069
5	Non-Cancerous images	26.4417	27.6548	32.9611	0.8575	0.4412	0.5855	0.0017	0.0068	0.0006
6	Cancerous images	26.0886	27.3342	32.6845	0.4940	0.4915	0.8040	0.0018	0.0021	0.0049
	Average	26.6229	27.7749	33.0347	0.7136	0.4506	0.6373	0.0451	0.0036	0.0019

As tabulated in the Table 3, DWTCoSAMP is the best when compared to other CS techniques like FFTCoSaMP and DCTCoSaMP. The average values of PSNR for DWTCoSAMP are 32.9763, 32.1498, and 28.7848 for different measurement matrices like 210 x 256, 180 x 256, and 155 x 256 respectively. Similarly The average values of PSNR for DCTCoSaMP are 27.7014 dB, 26.1703 dB, and 24.2075 dB for different measurement matrices like 210 x 256, 180 x 256, and 155 x 256 respectively.

Table 3. PSNR based comparison of different compressive sampling algorithms under different dimensions of measurement matrices

CS algorithms	S.N.	Measurement matrix MRI images	DWTCoSAMP			DCTCoSaMP			FFTCoSAMP		
			155 x 256	180 x 256	210 x 256	155 x 256	180 x 256	210 x 256	155 x 256	180 x 256	210 x 256
P S N R	1	Glioma Tumor images	29.4521	32.7025	32.9565	24.0214	26.4812	27.9552	29.4521	25.0786	26.7953
	2	Brain Tumor images	29.0123	31.8925	32.7034	24.1245	26.7891	27.3214	28.0123	24.9214	26.1371
	3	Brain Tumorless images	29.4358	32.1245	33.2316	23.9754	26.2471	27.7369	29.4358	24.1234	26.7877
	4	No Brain Tumor images	28.1245	32.1246	33.3209	23.8974	25.8974	28.2062	28.0245	25.3124	26.9530
	5	Non-cancerous images	27.8975	32.3791	32.9611	24.5687	25.4589	27.6548	27.8975	24.5698	26.4417
	6	Cancerous images	28.7864	31.6754	32.6845	24.6573	26.1478	27.3342	28.7864	25.1234	26.0886
Average PSNR			28.7848	32.1498	32.9763	24.2075	26.1703	27.7014	28.6014	24.8548	26.5339

Table 3 shows the PSNR based comparison of different compressive sampling algorithms under different sizes of measurement matrices like 155x256, 180x256, and 210x256. As well, the average values of PSNR for FFTCoSaMP are 27.7014 dB, 26.1703 dB, and 24.2075 dB for different measurement matrices like 210x256, 180x256, and 155x256 respectively. Similarly average values of SSIM for the same different measurement matrices is tabulated and compared in Table 4. Likewise, average values of RMSE for the same different set of measurement matrices are tabulated and compared in Table 5.

Table 4. SSIM based comparison of different compressive sampling algorithms under different dimensions of measurement matrices

CS Algorithms	S. N.	Measurement matrix MRI images	DWTCoSAMP			DCTCoSaMP			FFTCoSAMP		
			155 x 256	180 x 256	210 x 256	155 x 256	180 x 256	210 x 256	155 x 256	180 x 256	210 x 256
S S I M	1	Glioma Tumor Images	0.5645	0.5332	0.5938	0.4674	0.4744	0.4644	0.4650	0.5144	0.7021
	2	Brain Tumor Images	0.4919	0.7424	0.8423	0.4824	0.3914	0.4914	0.4754	0.5914	0.8534
	3	Brain Tumorless Images	0.4268	0.5453	0.5759	0.5251	0.5251	0.4251	0.5721	0.4251	0.4284
	4	No Brain Tumor Images	0.4611	0.5861	0.5891	0.4411	0.3911	0.4311	0.5411	0.5311	0.7264
	5	Non-Cancerous Images	0.4412	0.4855	0.5855	0.4342	0.4121	0.4412	0.4412	0.4412	0.8575
	6	Cancerous Images	0.4915	0.7940	0.8040	0.5115	0.4115	0.4915	0.4250	0.4915	0.4940
Average SSIM			0.4795	0.6144	0.6651	0.4769	0.4343	0.4574	0.4866	0.4991	0.6770

4. DISCUSSION

About 2000 MRI images like Glioma Tumor images, Brain Tumor images, Tumor-Less images, Cancerous images and Non Cancerous images are used for experimentation. For all these images, average PSNR values for DWTCoSAMP, DCTCoSaMP, FFTCoSaMP are 32.9763, and 27.7014, 26.5339 respectively for the measurement matrix of 210x256. Similarly, SSIM values for DWTCoSAMP, DCTCoSaMP, FFTCoSaMP are 0.6651, 0.4574, and 0.6770 respectively for measurement matrix 210x256. Lastly, RMSE values for DWTCoSAMP, DCTCoSaMP, and

FFTCoSaMP is 0.0017, 0.0034, and 0.0379 respectively for measurement matrix 210x256. In all data analysis made in different measurement matrices of 155x256, 180x256, and 210x255, CS technique DWTCoSaMP is the best compared to DCTCoSaMP and FFTCoSaMP and other CS techniques.

Figure 4 shows the bar chart for the various PSNR values of Table 3. Figure 5 shows the bar chart for the various SSIM values of Table 4. Figure 6 shows the bar chart for the various RMSE values of Table 5. The charts show that for all different measurement matrices, the DWTCoSaMP provides a best result when compared to other CS techniques of the literature survey as referred in various references. If the SSIM value is appearing towards 1(one) or higher the PSNR values towards 100 dB or lower the RMSE values towards 0 (zero), there is a very good and better improvement in the reconstruction of MRI with respect to sparsity and incomplete signal.

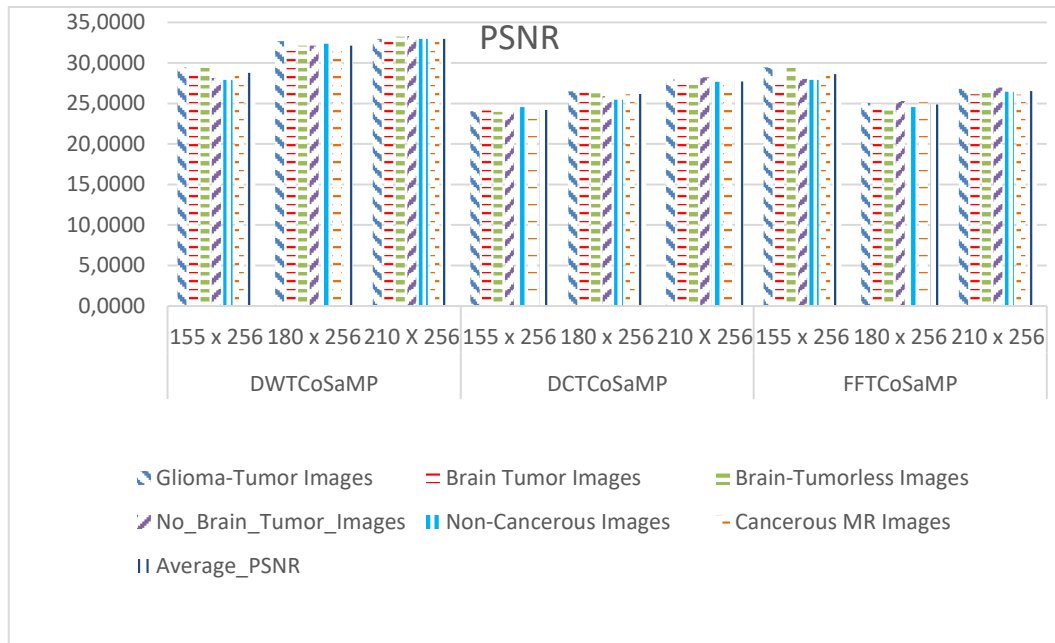


Figure 4. PSNR based bar chart for the analysis of FFTCoSaMP, DCTCoSaMP, and DWTCoSaMP

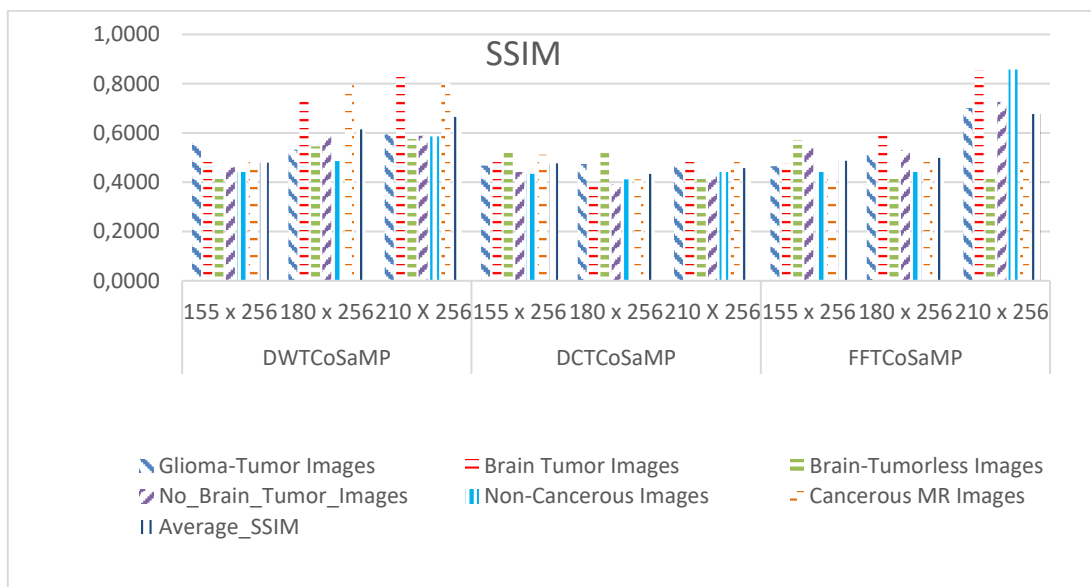


Figure 5. SSIM based bar chart for the analysis of FFTCoSaMP, DCTCoSaMP, and DWTCoSaMP

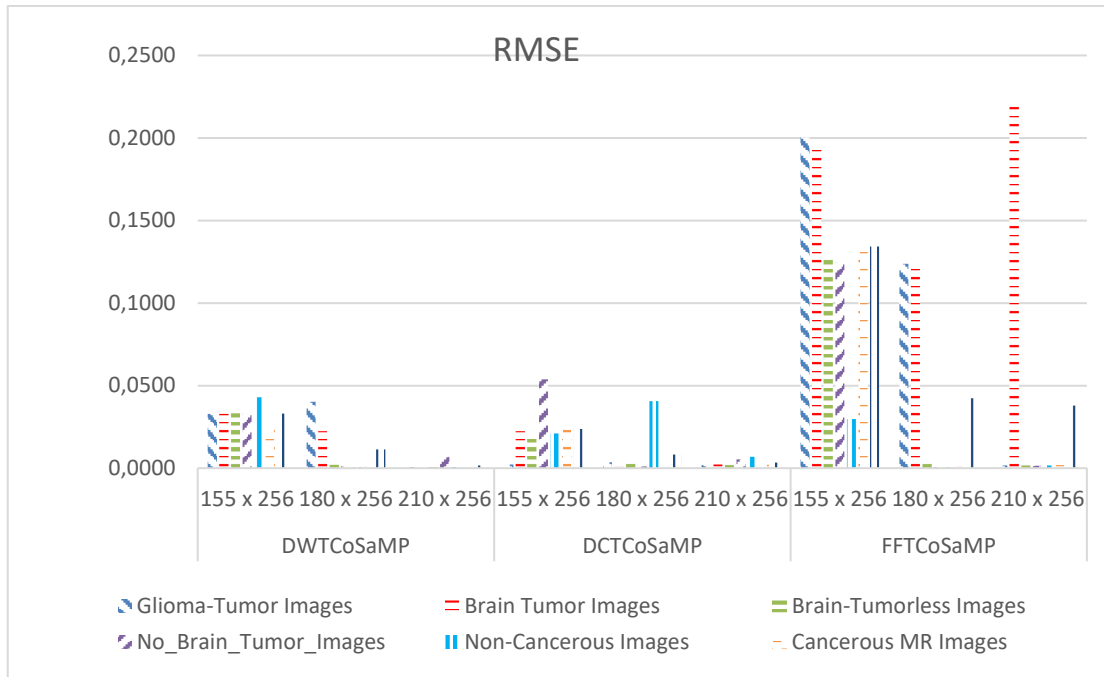


Figure 6. RMSE based bar chart for the analysis of FFTCoSaMP, DCTCoSaMP and DWTCoSAMP

Table 5. RMSE based comparison of different compressive sampling algorithms under different dimensions of measurement matrices

CS Algorithms	S. N.	Measurement matrix MRI images	DWTCoSAMP			DCTCoSaMP			FFTCoSAMP		
			155 x 256	180 x 256	210 x 256	155 x 256	180 x 256	210 x 256	155 x 256	180 x 256	210 x 256
R M S E	1	Glioma Tumor images	0.0329	0.0403	0.0006	0.0021	0.0036	0.0019	0.2004	0.1238	0.0016
	2	Brain Tumor images	0.0330	0.0223	0.0006	0.0224	0.0009	0.0021	0.1928	0.1237	0.2190
	3	Brain Tumorless images	0.0332	0.0021	0.0006	0.0192	0.0029	0.0019	0.1271	0.0049	0.0016
	4	No Brain Tumor images	0.0330	0.0013	0.0069	0.0539	0.0011	0.0053	0.1245	0.0004	0.0015
	5	Non-Cancerous images	0.0430	0.0005	0.0006	0.0210	0.0407	0.0068	0.0298	0.0005	0.0017
	6	Cancerous images	0.0236	0.0011	0.0006	0.0234	0.0005	0.0021	0.1314	0.0011	0.0018
Average RMSE			0.0331	0.0113	0.0017	0.0237	0.0083	0.0034	0.134	0.0424	0.0379

5. CONCLUSION

In this research work for exploitation of sparsity under different compressed sensing techniques, DWTCoSAMP reveals the best method when compared to DCTCoSaMP and FFTCoSaMP and other traditional methods. By varying the dimensionalities of measurement matrices, DWTCoSAMP gives best results when compared to DCTCoSaMP, FFTCoSaMP, and other traditional CS techniques. For my future study, we would like to work on audio and speech signal type of data. So, we would like to work on these datasets.

ACKNOWLEDGEMENTS

We like to thank Visvesvaraya Technological University (VTU), Gana Sangama, Belagavi, 590018, Karnataka, India for the monetary support extended to the research work.

REFERENCES

- [1] D. L. Donoho, "Compressed sensing," in *IEEE Transactions on Information Theory*, vol. 52, no. 4, pp. 1289-1306, Apr. 2006, doi: 10.1109/TIT.2006.871582.
- [2] E. P. Simoncelli, W. T. Freeman, E. H. Adelson and D. J. Heeger, "Shiftable multiscale transforms," in *IEEE Transactions on Information Theory*, vol. 38, no. 2, pp. 587-607, March 1992, doi: 10.1109/18.119725.
- [3] B. P. V. Dileep, T. Das, and K. Dutta, "Greedy algorithms for diffuse optical tomography reconstruction," *Optics Communications*, vol. 410, no. 1, pp. 164-173, Mar. 2018, doi: 10.1016/j.optcom.2017.09.056.
- [4] B. P. V. Dileep, T. Das, and K. Dutta, "Sparse recovery based compressive sensing algorithms for diffuse optical tomography," *Optics & Laser Technology*, vol. 128, p. 106234, Aug. 2020, doi: 10.1016/j.optlastec.2020.106234.
- [5] Y. Liu, X. Chen, A. Liu, R. K. Ward, and Z. J. Wang, "Recent advances in sparse representation based medical image fusion," in *IEEE Instrumentation & Measurement Magazine*, vol. 24, no. 2, pp. 45-53, April 2021, doi: 10.1109/MIM.2021.9400960.
- [6] E. Candes and J. Romberg, "Sparsity and incoherence in compressive sampling," *Inverse Problems*, vol. 23, no. 3, p. 969, Apr. 2007.
- [7] M. Lustig, D. Donoho, and J. M. Pauly, "Sparse MRI: the application of compressed sensing for rapid MR imaging," *Magnetic Resonance in Medicine*, vol. 58, no. 6, pp. 1182-1195, Oct. 2007, doi: 10.1002/mrm.21391.
- [8] Y. V. Parkale and S. L. Nalbalwar, "Application of compressed sensing for image compression based on optimized Toeplitz sensing matrices," *EURASIP Journal on Advances in Signal Processing*, vol. 70, no. 1, pp. 1-30, 2021, doi: 10.1186/s13634-021-00743-5.
- [9] Q. Deng *et al.*, "Compressed sensing for image reconstruction via back-off and rectification of greedy algorithm," *Signal Processing*, vol. 157, pp. 280-287, 2019, doi: 10.1016/j.sigpro.2018.12.007.
- [10] Y. Fang, L. Li, Y. Li, H. Peng, and Y. Yang, "Low energy consumption compressed spectrum sensing based on channel energy reconstruction in cognitive radio network," *Sensors*, vol. 20, no. 5, p. 1264, Feb. 2020, doi: 10.3390/s20051264.
- [11] D. Ba, "Deeply-Sparse Signal rePresentations (DS2P)," in *IEEE Transactions on Signal Processing*, vol. 68, pp. 4727-4742, 2020, doi: 10.1109/TSP.2020.3014716.
- [12] P. Heckbert, "Fourier transforms and the fast fourier transform (FFT) algorithm," *Computer Graphics* 2, 1995, pp. 15-463.
- [13] J. Dong, H. Li, Z. Fan, and X. Zhao, "Time-frequency sparse reconstruction of non-uniform sampling for non-stationary signal," in *IEEE Transactions on Vehicular Technology*, vol. 70, no. 11, pp. 11145-11153, Nov. 2021, doi: 10.1109/TVT.2021.3111213.
- [14] A. Y. Carmi, L. S. Mihaylova, and S. J. Godsill, *Compressed sensing and sparse filtering and communication technology*, Springer-Verlag Berlin Heidelberg 2014, doi: 10.1007/978-3-642-38398-4.
- [15] H. J. Landau, "Sampling, data transmission, and the Nyquist rate," in *Proceedings of the IEEE*, vol. 55, no. 10, pp. 1701-1706, Oct. 1967, doi: 10.1109/PROC.1967.5962.
- [16] E. J. Candes and M. B. Wakin, "An introduction to compressive sampling," in *IEEE Signal Processing Magazine*, vol. 25, no. 2, pp. 21-30, March 2008, doi: 10.1109/MSP.2007.914731.
- [17] N. Ahmed, T. Natarajan, and K. R. Rao, "Discrete Cosine Transform," in *IEEE Transactions on Computers*, vol. C-23, no. 1, pp. 90-93, Jan. 1974, doi: 10.1109/T-C.1974.223784.
- [18] C. A. Chalaperumal and S. D. kumar, "An efficient image quality enhancement using wavelet transform," *Materials Today: Proceedings*, vol. 24, pp. 2004-2010, 2020, doi: 10.1016/j.matpr.2020.03.629.
- [19] M. Junge and K. Lee, "Generalized notions of sparsity and restricted isometry property. Part I: a unified framework," *Information and Inference: A Journal of the IMA*, vol. 9, no. 1, pp. 157-193, Mar. 2020, doi: 10.1093/imaia/iy018.
- [20] J.-F. Cai, J. Li, X. Lu, and J. You, "Sparse signal recovery from phaseless measurements via hard thresholding pursuit," *Applied and Computational Harmonic Analysis*, vol. 56, pp. 367-390, Jan. 2022, doi: 10.1016/j.acha.2021.10.002.
- [21] J. Li, "Effective phase retrieval of sparse signals with convergence guarantee," *Signal Processing*, vol. 192, p. 108388, Mar. 2022, doi: 10.1016/j.sigpro.2021.108388.
- [22] E. J. Candes, J. Romberg, and T. Tao, "Robust uncertainty principles: exact signal reconstruction from highly incomplete frequency information," in *IEEE Transactions on Information Theory*, vol. 52, no. 2, pp. 489-509, Feb. 2006, doi: 10.1109/TIT.2005.862083.
- [23] E. J. Candes and T. Tao, "Near-optimal signal recovery from random projections: universal encoding strategies?," in *IEEE Transactions on Information Theory*, vol. 52, no. 12, pp. 5406-5425, Dec. 2006, doi: 10.1109/TIT.2006.885507.
- [24] J. A. Tropp and A. C. Gilbert, "Signal recovery from random measurements via orthogonal matching pursuit," in *IEEE Transactions on Information Theory*, vol. 53, no. 12, pp. 4655-4666, Dec. 2007, doi: 10.1109/TIT.2007.909108.
- [25] D. Needell and J. A. Tropp, "CoSaMP: iterative signal recovery from incomplete and inaccurate samples, applied and computational harmonic analysis," *Applied and Computational Harmonic Analysis*, vol. 26, no. 3, pp. 301-321, May 2009, doi: 10.1016/j.acha.2008.07.002.
- [26] D. Lu, G. Sun, Z. Li, and S. Wang, "Improved CoSaMP reconstruction algorithm based on residual update," *Journal of Computer and Communications*, vol. 7 no. 6, p. 6, 2019, doi: 10.4236/jcc.2019.76002.
- [27] P. Zhang, B. Ba, Y. Zhang, and P. Han, "Sparse reconstruction off-grid OFDM time delay estimation algorithm based on bayesian automatic relevance determination," *Journal of Physics: Conference Series*, vol. 1237, no. 2, p. 022096, Jun. 2019.
- [28] Z. Meng, G. Zhang, Z. Pan, W. Gao, H. Gao, and F. Fan, "A sparse measurement matrix based method for feature enhancement of bearing fault signal," *Applied Acoustics*, vol. 177, p. 107903, Jun. 2021, doi: 10.1016/j.apacoust.2020.107903.
- [29] M. D. Deepak, P. Karthik, S. S. Kumar, and N. A. Deepak, "Comparative study of feature extraction using different transform techniques in frequency domain," *Advances in Automation, Signal Processing, Instrumentation, and Control*, vol. 700, pp. 2835-2846, 2021, doi: 10.1007/978-981-15-8221-9_265.
- [30] Y. Zhang, D. Wang, L. Kan, and P. Zhao, "A study on image reconfiguration algorithm of compressed sensing," *TELKOMNIKA Telecommunication, Computing, Electronics and Control*, vol. 15, no. 1, pp. 299-305, Mar. 2017, doi: 10.12928/TELKOMNIKA.v15i1.3710.
- [31] Hui-Huang Zhao, P. L. Rosin, Yu-Kun Lai, Jin-Hua Zheng, and Yao-Nan Wang, "Adaptive gradient-based block compressive sensing with sparsity for noisy images," *Multimedia Tools and Applications* vol. 79, pp. 14825-14847, 2022, doi: 10.1007/s11042-019-7647-8.
- [32] J. Cheng, "An improved off-grid algorithm based on CoSaMP for ISAR imaging," *2020 5th International Conference on Mechanical, Control and Computer Engineering (ICMCCE)*, 2020, pp. 1643-1646, doi: 10.1109/ICMCCE51767.2020.00360.
- [33] Z. Wu, J. Sha, Z. Wang, L. Li, and M. Gao, "An improved scaled DCT architecture," in *IEEE Transactions on Consumer Electronics*, vol. 55, no. 2, pp. 685-689, May 2009, doi: 10.1109/TCE.2009.5174440.
- [34] E. Crespo Marques, N. Maciel, L. Naviner, H. Cai and J. Yang, "A Review of Sparse Recovery Algorithms," in *IEEE Access*, vol. 7, pp. 1300-1322, 2019, doi: 10.1109/ACCESS.2018.2886471.
- [35] X. Bi, L. Leng, C. Kim, X. Liu, Y. Du, and F. Liu, "Constrained backtracking matching pursuit algorithm for image reconstruction in compressed sensing," *Applied Sciences*, vol. 11, no. 4, p. 1435, Feb. 2021, doi: 10.3390/app11041435.

- [36] M. A. Baig, A. A. Moinuddin, and E. Khan, "PSNR of highest distortion region: an effective image quality assessment method," *2019 International Conference on Electrical, Electronics and Computer Engineering (UPCON)*, 2019, pp. 1-4, doi: 10.1109/UPCON47278.2019.8980171.
- [37] J. D. Villasenor, B. Belzer and J. Liao, "Wavelet filter evaluation for image compression," in *IEEE Transactions on Image Processing*, vol. 4, no. 8, pp. 1053-1060, Aug. 1995, doi: 10.1109/83.403412.
- [38] T. S. Kavita and K. S. Prasad, "Quantitative comparison of reconstruction methods for compressive sensing MRI," *International Journal Of Scientific & Technology Research*, vol. 8, no. 10, pp. 1504-1507, Oct. 2019.

BIOGRAPHIES OF AUTHORS



Deepak M. Devendrappa    is a research scholar in the Department of Computer Science and Engineering, at K S School of Engineering and Management, Bengaluru, from Visvesvaraya Technological University Belagavi. He can be contacted at email: mddeepak1986@gmail.com.



Karthik P.    has received the Ph.D. Degree in the Department of Electronics and Communication Engineering. He is presently working as Professor in the Department of ECE at K S School of Engineering and Management, Bengaluru. He has more than 10 years of experience in teaching and has published papers in 4 International Journals, 3 International Conferences and 4 National Conferences. He has done about 19 journal and research articles in 20 international and 20 national conferences. His areas of specialization are embedded systems, networks, and communication. He is a senior IEEE member. He can be contacted at email: karthik.p@kssem.edu.in.



Deepak N. Ananth    received his doctoral degree in 2017 and currently working as an Associate Professor, in Department of Computer Science and Engineering, at RV Institute of Technology and Management, Bengaluru. He has 20 of teaching experience at reputed Engineering colleges and has 6 years of research experience at National Aerospace Laboratories, Bengaluru, Karnataka. His area of interest includes machine learning, deep learning, and signal processing. He can be contacted at email: deepak.n.ananth@gmail.com.



Aruna Kumar P.    is working as Assistant Professor in the Department of Information science and Engineering, at J N N College of Engineering, Shivamogga, India. He can be contacted at email: arunkumar.p@jnnce.ac.in.